

## Article

# Trivalent Ions and Their Impacts on Effective Conductivity at 300 K and Radio-Protective Behaviors of Bismo-Borate Glasses: A Comparative Investigation for Al, Y, Nd, Sm, Eu

Ghada ALMisned<sup>1</sup>, Huseyin O. Tekin<sup>2,3,\*</sup>, Ghaida Bilal<sup>2,4</sup>, Antoaneta Ene<sup>5,\*</sup>, Gokhan Kilic<sup>6</sup>,  
Shams A. M. Issa<sup>7,8</sup>, Merfat Algethami<sup>9</sup> and Hesham M. H. Zakaly<sup>8,10,\*</sup>

<sup>1</sup> Department of Physics, College of Science, Princess Nourah Bint Abdulrahman University, Riyadh 11671, Saudi Arabia; gaalmisned@pnu.edu.sa

<sup>2</sup> Medical Diagnostic Imaging Department, College of Health Sciences, University of Sharjah, Sharjah 27272, United Arab Emirates; u17104268@sharjah.ac.ae

<sup>3</sup> Medical Radiation Research Center (USMERA), Uskudar University, 34672 Istanbul, Turkey

<sup>4</sup> Center for Advanced Materials Research, Research Institute of Sciences and Engineering, University of Sharjah, Sharjah 27272, United Arab Emirates

<sup>5</sup> INPOLDE Research Center, Department of Chemistry, Physics and Environment, Faculty of Sciences and Environment, Dunarea de Jos University of Galati, 47 Domneasca Street, 800008 Galati, Romania

<sup>6</sup> Department of Physics, Faculty of Science and Letters, Eskisehir Osmangazi University, 26040 Eskisehir, Turkey; gkilic@ogu.edu.tr

<sup>7</sup> Physics Department, Faculty of Science, University of Tabuk, Tabuk 47512, Saudi Arabia; sh\_issa@ut.edu.sa

<sup>8</sup> Physics Department, Faculty of Science, Al-Azhar University, Assiut 71524, Egypt

<sup>9</sup> Physics Department, Faculty of Science, Taif University, Taif, P. O. Box 11099, Taif 21944, Saudi Arabia; M.algethami@tu.edu.sa

<sup>10</sup> Institute of Physics and Technology, Ural Federal University, 620002 Ekaterinburg, Russia

\* Correspondence: htekin@sharjah.ac.ae (H.O.T.); Antoaneta.Ene@ugal.ro (A.E.); h.m.zakaly@azhar.edu.eg (H.M.H.Z.)



**Citation:** ALMisned, G.; Tekin, H.O.; Bilal, G.; Ene, A.; Kilic, G.; Issa, S.A.M.; Algethami, M.; Zakaly, H.M.H. Trivalent Ions and Their Impacts on Effective Conductivity at 300 K and Radio-Protective Behaviors of Bismo-Borate Glasses: A Comparative Investigation for Al, Y, Nd, Sm, Eu. *Materials* **2021**, *14*, 5894. <https://doi.org/10.3390/ma14195894>

Academic Editor:  
Gianfranco Dell'Agli

Received: 20 August 2021  
Accepted: 6 October 2021  
Published: 8 October 2021

**Publisher's Note:** MDPI stays neutral with regard to jurisdictional claims in published maps and institutional affiliations.



**Copyright:** © 2021 by the authors. Licensee MDPI, Basel, Switzerland. This article is an open access article distributed under the terms and conditions of the Creative Commons Attribution (CC BY) license (<https://creativecommons.org/licenses/by/4.0/>).

**Abstract:** We aimed to determine the contribution of various trivalent ions like Al and rare-earths (Y, Nd, Sm, Eu) on resistance behaviors of different types of bismo-borate glasses. Accordingly, eight different bismuth borate glasses from the system:  $40\text{Bi}_2\text{O}_3-59\text{B}_2\text{O}_3-1\text{Tv}_2\text{O}_3$  (where  $\text{Tv} = \text{Al, Y, Nd, Sm, and Eu}$ ) and three glasses of  $(40\text{Bi}_2\text{O}_3-60\text{B}_2\text{O}_3; 37.5\text{Bi}_2\text{O}_3-62.5\text{B}_2\text{O}_3; \text{ and } 38\text{Bi}_2\text{O}_3-60\text{B}_2\text{O}_3-2\text{Al}_2\text{O}_3)$  compositions were extensively investigated in terms of their nuclear attenuation shielding properties, along with effective conductivity and buildup factors. The Py-MLBUF online platform was also utilized for determination of some essential parameters. Next, attenuation coefficients, along with half and tenth value layers, have been determined in the 0.015 MeV–15 MeV photon energy range. Moreover, effective atomic numbers and effective atomic weight, along with exposure and energy absorption buildup factors, were determined in the same energy range. The result showed that the type of trivalent ion has a direct effect on behaviors of bismo-borate glasses against ionizing gamma-rays. As incident photon energy increases, the effective thermal conductivity decreases rapidly, especially in the low energy range, where photoelectric effects dominate the photon–matter interaction. Sample 8 had the minimum heat conductivity at low photon energies; our findings showed that Eu-reinforced bismo-borate glass composition, namely  $40\text{Bi}_2\text{O}_3-59\text{B}_2\text{O}_3-1\text{Eu}_2\text{O}_3$ , with a glass density of  $6.328 \text{ g/cm}^3$  had superior gamma-ray attenuation properties. These outcomes would be useful for the scientific community to observe the most suitable additive rareearth type and related glass composition for providing the aforementioned shielding properties, in terms of needs and utilization requirements.

**Keywords:** bismo-borate glasses; trivalent ions; rare-earth; effective conductivity; Py-MLBUF; radiation shielding

## 1. Introduction

Over the past few decades, radiation has become one of the most significant research topics. Over time, scientists have gained a better understanding of the potential for biological harm caused by various forms and characteristics of radiation. The most widely used classification system for categorizing radiation according to its potential to cause damage to living tissue divides it into two groups: ionizing and non-ionizing radiation. Ionizing radiation has come a long way in terms of widespread use and widely spreading its destructive effects on biological structures and living cells through direct or indirect effects [1]. It is important to protect people from the harmful effects of ionizing radiation. The word “radiation safety” has gained even more significance as a result of the application of radiation sciences in a variety of high-tech fields. For several years, certain traditional nuclear shielding materials have been used in some radiation fields based on use attributes [2]. Because of its low cost, easy availability, and ability to be shaped into any shape or form, concrete is the most commonly used shielding material [3,4] in nuclear reactors and cyclotrons. Concrete, however, has a number of drawbacks, which include cracks that appear after prolonged use, and the presence of water in concrete that reduces the material’s density and structural strength. Moreover, concrete is opaque by nature, making it difficult to see through. In the recent years, researchers have been trying to investigate the features of materials that can be utilized as a replacement for concrete and lead [5]—ones that are eco-friendly, highly dense, and chemically homogenous. Various materials, such as compounds, steel [6,7], and alloys [8–11] have been chosen and tested for their shielding applications in order to investigate the desired features. The findings revealed that strong, nontransparent concrete and lead outperform, prompting scientists to research glass systems to serve as radiation shielding materials. The precise composition of a glass can differ to meet the needs of certain applications. A typical glass can be described as clear, non-toxic, and usable with advanced material characteristics for a variety of purposes. Recent attention has been focused on glass samples doped with rare-earth elements, which show promise for a variety of applications, including optical amplifiers, laser instruments, and radiation shields. Glass samples with a higher concentration of bridging oxygen are critical for radiation shielding and mechanical properties [12–14]. The high density and optical transparency of glasses containing heavy metals such as Eu (Z-63), Sm (Z-62) and Nd (Z-60) make them ideal for radiation shielding applications [15–17]. Aluminum oxide and yttrium serve as modifiers due to their elemental mass fractions in glass samples. Bismuth oxide, on the other hand, has a significant density and refractive index advantage [18–20]. Yttria, a boro-bismuthate [21,22]-doped material that is used to control the arrangement of glass, is more valuable than borate or phosphate glass [23–25]. Additionally, it exhibits exceptional chemical and photochemical stability, in addition to highly evolved properties. The literature review, on the other hand, showed that the importance of  $\text{Al}_2\text{O}_3$  has been investigated in terms of its critical properties. In a study, Popov et al. have compared thermal annealing of the F-type center in  $\text{Al}_2\text{O}_3$  single crystals irradiated with heavy ions and neutrons [26]. Moreover, Kotomin et al. have investigated the kinetics of F center as well as colloid creation in  $\text{Al}_2\text{O}_3$  [27]. As is well recognized,  $\text{Al}_2\text{O}_3$  is of considerable importance due to its material characteristics. In another study, Tucker et al. have investigated the effects of neutron-irradiation on  $\text{Al}_2\text{O}_3$  [28]. The present concept of these promising investigations has prompted us to do further research on the impact of other reinforcement types, including  $\text{Al}_2\text{O}_3$ , on the gamma-ray shielding properties of bismo-borate glasses. The aim of this study is to look into the nuclear shielding properties of various trivalent element oxides like  $\text{Al}_2\text{O}_3$  and some rare-earth oxide-doped ( $\text{Y}^{3+}$ ,  $\text{Sm}^{3+}$ ,  $\text{Nd}^{3+}$ ,  $\text{Eu}^{3+}$ ) glass samples, using the Python multilayered buildup factor (Py-MLBUF) online platform [29] for energies between 0.015 and 15 MeV. Boro-bismuthate was chosen as the basic glass sample for this study due to its exceptional shielding and clarity properties. It should be noted that the results of this study will be applicable to the field of glass literature, particularly radiation shielding. In addition, the obtained findings can be used to evaluate the composition of rare-earth-doped boro-bismuthate glass in recent amorphous structures

on a broad scale. The results of this research could help researchers better understand the suitability of rare-earth doped glass samples as nuclear shielding materials.

## 2. Materials and Methods

In this study, eight different bismuth borate glass systems [30] were extensively investigated in terms of their nuclear attenuation shielding properties, along with their effective conductivity and buildup factors. The chemical composition of the studied glasses can be defined as below.

- (i) 37.5Bi<sub>2</sub>O<sub>3</sub>–62.5B<sub>2</sub>O<sub>3</sub>
- (ii) 38Bi<sub>2</sub>O<sub>3</sub>–60B<sub>2</sub>O<sub>3</sub>–2Al<sub>2</sub>O<sub>3</sub>
- (iii) 40Bi<sub>2</sub>O<sub>3</sub>–60B<sub>2</sub>O<sub>3</sub>
- (iv) 40Bi<sub>2</sub>O<sub>3</sub>–59B<sub>2</sub>O<sub>3</sub>–1Al<sub>2</sub>O<sub>3</sub>
- (v) 40Bi<sub>2</sub>O<sub>3</sub>–59B<sub>2</sub>O<sub>3</sub>–1Y<sub>2</sub>O<sub>3</sub>
- (vi) 40Bi<sub>2</sub>O<sub>3</sub>–59B<sub>2</sub>O<sub>3</sub>–1Nd<sub>2</sub>O<sub>3</sub>
- (vii) 40Bi<sub>2</sub>O<sub>3</sub>–59B<sub>2</sub>O<sub>3</sub>–1Sm<sub>2</sub>O<sub>3</sub>
- (viii) 40Bi<sub>2</sub>O<sub>3</sub>–59B<sub>2</sub>O<sub>3</sub>–1Eu<sub>2</sub>O<sub>3</sub>

In the reference study, material densities of glass samples were reported as 6.006 g/cm<sup>3</sup>, 6.07 g/cm<sup>3</sup>, 6.313 g/cm<sup>3</sup>, 6.233 g/cm<sup>3</sup>, 6.301 g/cm<sup>3</sup>, 6.341 g/cm<sup>3</sup>, 6.321 g/cm<sup>3</sup>, 6.328 g/cm<sup>3</sup> for Sample 1, Sample 2, Sample 3, Sample 4, Sample 5, Sample 6, Sample 7 and Sample 8, respectively (see Table 1). In this section, we will present the determined nuclear radiation shielding parameters along with their technical details. Moreover, we will present a brief definition of the used Py-MLBUF online platform.

**Table 1.** The codes, elemental compositions, weight fractions and densities of the studied glass samples.

Sample Code	B	O	Bi	Al	Y	Nd	Sm	Eu	Density (g/cm <sup>3</sup> )
1	0.061915	0.219923	0.718162	-	-	-	-	-	6.006
2	0.058731	0.217306	0.719077	0.004886	-	-	-	-	6.07
3	0.056857	0.210372	0.732771	-	-	-	-	-	6.313
4	0.05583	0.210074	0.731734	0.002362	-	-	-	-	6.233
5	0.055529	0.208942	0.727789	-	0.007741	-	-	-	6.301
6	0.055263	0.20794	0.7243	-	-	0.012498	-	-	6.341
7	0.055233	0.20783	0.723916	-	-	-	0.013021	-	6.321
8	0.05523	0.20780	0.72382	-	-	-	-	0.00658	6.328

### 2.1. Nuclear Radiation Shielding Parameters

It is essential to comprehend the Lambert–Beer law [31,32], shown in Equation (1), to simplify the mass attenuation coefficient.

$$I = I_0 e^{-\mu t} \quad (1)$$

I: Intensity of the secondary gamma rays

I<sub>0</sub>: Intensity of the initial gamma rays

μ: Linear attenuation coefficient

t: Thickness of the absorber

The mass attenuation coefficient (g/cm<sup>3</sup>) [33,34] is a measure of how likely incident photons are to interact with matter per unit density. It is calculated using the formula demonstrated in Equation (2):

$$\mu/\rho = \sum_i w_i (\mu/\rho)_i \quad (2)$$

where μ (1/cm) is the linear attenuation coefficient, and ρ is the density of the sample, w<sub>i</sub> is the weight fraction of the i<sup>th</sup> constituent of the element. The Mean Free Path (MFP cm) [35]

is the average distance traveled by photons before collision. For any photon passing through a material, MFP is calculated using Equation (3):

$$\text{MFP} = \frac{1}{\mu} \quad (3)$$

After traveling 1 mfp through a shielding medium in an ideal narrow-beam geometry, the power of monoenergetic gamma-rays is reduced by approximately 37%. By multiplying the linear attenuation coefficient by the distance in cm between the point source and the detector, a dimensionless quantity is obtained. The term "optical thickness (OT)" refers to this dimensionless quantity. When gamma-photons traverse the shield, the OT shows how many mean free path lengths they completed. Half Value Layers (HVL cm) is described as the absorber thickness necessary to eliminate the radiation intensity to half its original value. It is calculated using Equation (4):

$$\text{HVL} = \frac{\ln(2)}{\mu} \quad (4)$$

Another metric that is comparable to HVL cm [36,37] is the Tenth Value Layer (TVL cm), which is defined as the thickness of absorber required to decrease the radiation intensity to one-tenth of its original value. It is computed using the following Equation (5):

$$\text{TVL} = \frac{\ln(10)}{\mu} \quad (5)$$

The effective conductivity  $C_{\text{eff}}$  (s/m) [38] of a shielding-material for attenuation at room temperature (300 K) is related to the effective number of electrons ( $N_{\text{eff}}$ ) by the following Equation (6):

$$C_{\text{eff}} = \left( \frac{N_{\text{eff}} \rho e^2 \tau}{m_e} \right) \times 10^3 \quad (6)$$

In Equation (7),  $\rho$ ,  $e$  and  $m_e$  denote the density of shielding materials ( $\text{g}\cdot\text{cm}^{-3}$ ), the charge on an electron (C), and the electron's rest mass (kg), respectively.  $\tau$  depicts the electron's relaxation time and is calculated using the following equation:

$$\tau = \frac{h}{600\pi k} \quad (7)$$

where  $h$  is Planck's constant and  $k$  is the Boltzmann constant. In radiation studies, the term  $Z_{\text{eff}}$  is a crucial parameter. The effective atomic number function can also be used to characterize the improvement of shielding in complex shielding materials. The effective atomic number was determined in this research using the direct method of examining the atomic and electronic cross sections.

$$Z_{\text{eff}} = \frac{\sum_i f_i A_i \left( \frac{\mu}{\rho} \right)_i}{\sum_j f_j \left( \frac{A_j}{Z_j} \right) \left( \frac{\mu}{\rho} \right)_j} \quad (8)$$

where  $f_i$ : fraction by mole

$A_i$ : atomic weight

$Z_j$ : Atomic number of  $i$ th constituent element

The atomic number ( $Z_{\text{eq}}$ ) of a shielding material is assigned exclusively by incoherent scattering. Values of  $Z_{\text{eq}}$  aid in buildup factor (BUF) calculations.

$Z_{\text{eq}}$  values in this study were obtained using the interpolation method, demonstrated in Equation (9):

$$Z_{\text{eq}} = \frac{Z_1(\log R_2 - \log R) + Z_2(\log R - \log R_1)}{\log R_2 - \log R_1} \quad (9)$$

where the ratio  $R$  is the determining factor for the equivalent atomic number, for a particular photon energy.

$$R = \frac{\mu_{m \text{ Compton}}}{\mu_{m \text{ total}}} \quad (10)$$

$Z_1$  and  $Z_2$  are the atomic numbers of the respective elements, which correspond to their respective ratios  $R_1$  and  $R_2$ . The buildup factor is a multiplicative factor that takes into account the contributions of scattered photons to the corrected response to uncollided photons. In simpler terms, it is the ratio of incident photons to total photons. The ANS-standard was developed to compute gamma-ray BUFs for a point isotropic source operating between 0.015 and 15 MeV. The energy absorption build-up factor is a factor in which the quantity of interest is the amount of energy absorbed or stored in the interacting material. The geometric progression (G-P) fitting technique is often used to log EABFs. In this study, Py-MLBUF has been used for exposure (EBF) and energy absorption (EABF) buildup factors.

## 2.2. Python Multilayered (Py-MLBUF) Online Platform

Py-MLBUF [26] is a simple-to-use online calculator for determining gamma shielding parameters (GSP). Designed to measure the sum, 36 GSP (gamma shielding parameters) is used for gamma shielding enclosures used in radiation protection with an energy range of 0.015–15 MeV. This online platform's feedback system was developed in the form of a question–answer format. Following sign-in, the user is prompted for the number of layers ( $n$ ) in the GSE (gamma shielding energy), which is set to one for the sake of this study. The second issue concerns the composition form of the sample, which can be either elemental or compound; in this case, an elemental composition was chosen. The OT's maximum value is set to 40 mfp by default. The energy range chosen for this analysis was 0.015–15 MeV. Last but not least, the densities and weight fractions of each substance were entered. After that, the platform calculates all of the required shielding parameters, such as MAC—mass attenuation coefficient, LAC—Linear attenuation coefficient, BUFs—buildup factor,  $Z_{eq}$ — $Z$  equivalent,  $Z_{eff}$ —effective atomic number, HVL, TVL, and so on.

## 3. Results and Discussion

The shielding properties of eight high-density glass samples were determined in terms of their gamma-ray attenuation competencies in this study. Figure 1 shows the linear attenuation coefficients ( $\mu$ ) of glass samples, which vary in accordance with the photon energy; the energy range is from 0.015 to 15 MeV. There are two distinct ways to get energy for photons, and both techniques need the use of electrons. Absorption may vary in two different cases: In one instance, the photon is fully absorbed; in the other, only a portion of the light is absorbed, with the remainder being scattered. There is a direct relationship between the probability of these events occurring and the temperature and photon capacity of the medium. For low-energy photons, the photoelectric effect appears to be stronger (less than 100 keV); it grows to a higher probability of occurrence as  $Z$  increases. When the energy of photons is between moderate and high, the Compton effect is significant (more than 100 keV). When an electron's energy is more than 1.02 MeV, it will form a pair with a photon. Due to these numerous interactions, the linear attenuation coefficient may be concluded to be energy-dependent and to vary with different photon energy regions.

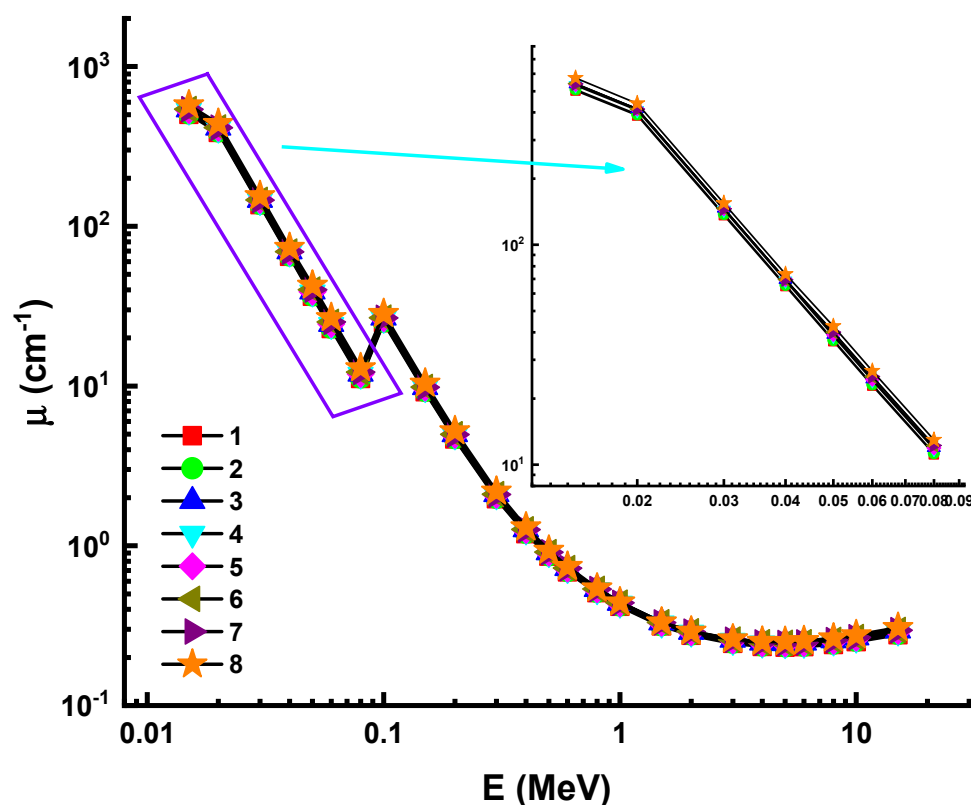


**Figure 1.** Variation of linear attenuation coefficient ( $\mu$ ) against Photon energy for all glasses.

In Figure 1, a fast drop of 0.015 MeV to 0.08 MeV was observed. As was the case with the first field, a smooth decrement was observed in the second, demonstrating Compton scattering's supremacy. Our results indicate that for the measured Sample 8, the highest values were discovered. This can be explained by the Eu reinforcement ( $Z = 63$ ) amount in Sample 8. As is seen in Table 1, Eu-reinforced Sample 8 has almost the maximum glass density (i.e.,  $6.328 \text{ g/cm}^3$ ). This is due to the higher atomic number of Eu compared to other additive types such as Al, Y, Nd, and Sm.

In the other hand, it might be more efficient to express the attenuation rate in terms of the mass of the photon-experienced target, rather than a radius. The factor affecting the attenuation rate is not the overall mass of the attenuator, but rather the region mass [39,40]. The simplest description of this phenomenon is in terms of mass attenuation coefficients ( $\mu_m$ ).  $\mu_m$  is a density-independent quantity that can be used to quantify a material's shielding abilities. The  $\mu_m$  values of the samples were calculated in the 0.015 MeV and 15 MeV photon energy ranges in this analysis. The distribution of  $\mu_m$  as a function of incident photon energy is depicted in Figure 2 for all glasses;  $\mu_m$  values reported a similar attitude toward  $m$ . Additionally, the predominance of the above interactions was stated in terms of  $\mu_m$  values. This relation is due to the seamless transitions between the densities of glass samples. Due to the fact that  $\mu_m$  can be found by dividing by density, a similar variance pattern is predicted. However, Sample 8 had the highest  $\mu_m$  values among the studied samples. This may be because the total mass of Sample 8 was closely related to the Eu's  $Z$  value.

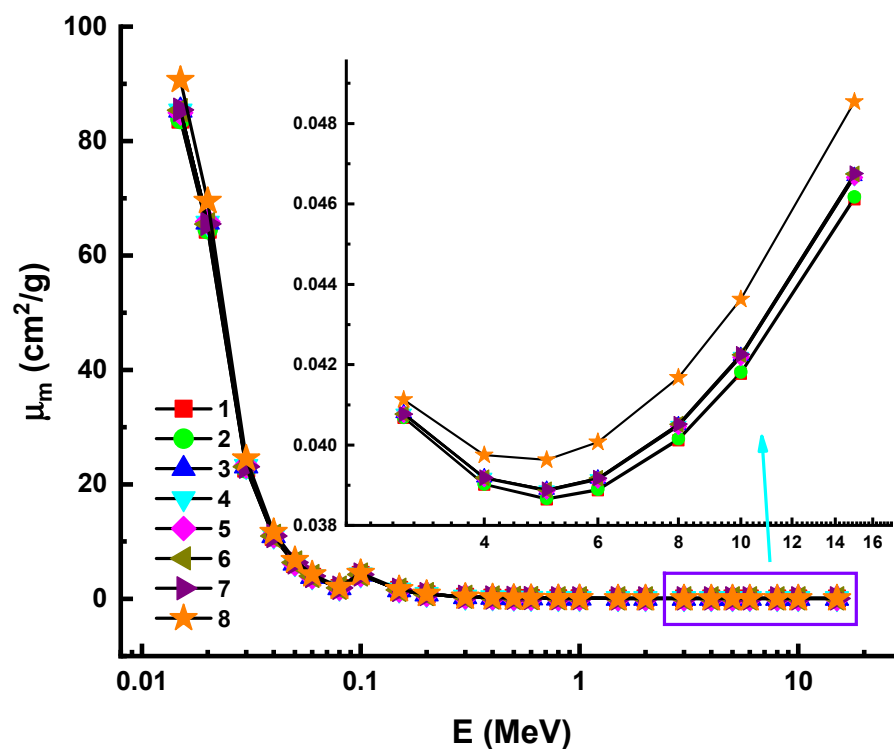


**Figure 2.** Variation of mass attenuation coefficient ( $\mu_m$ ) against photon energy for all glasses. 1— $37.5\text{Bi}_2\text{O}_3\text{--}62.5\text{B}_2\text{O}_3$ ; 2— $38\text{Bi}_2\text{O}_3\text{--}60\text{B}_2\text{O}_3\text{--}2\text{Al}_2\text{O}_3$ ; 3— $40\text{Bi}_2\text{O}_3\text{--}60\text{B}_2\text{O}_3$ ; 4— $40\text{Bi}_2\text{O}_3\text{--}59\text{B}_2\text{O}_3\text{--}1\text{Al}_2\text{O}_3$ ; 5— $40\text{Bi}_2\text{O}_3\text{--}59\text{B}_2\text{O}_3\text{--}1\text{Y}_2\text{O}_3$ ; 6— $40\text{Bi}_2\text{O}_3\text{--}59\text{B}_2\text{O}_3\text{--}1\text{Nd}_2\text{O}_3$ ; 7— $40\text{Bi}_2\text{O}_3\text{--}59\text{B}_2\text{O}_3\text{--}1\text{Sm}_2\text{O}_3$ ; 8— $40\text{Bi}_2\text{O}_3\text{--}59\text{B}_2\text{O}_3\text{--}1\text{Eu}_2\text{O}_3$ .

The term HVL ( $T_{1/2}$ ) is important for calculating the shield thickness of a material, since it may decrease the incoming photon intensity to half its value (as 50 percent). Thus, this configuration method may be utilized to account for future practical considerations such as the optimum physical environment for shielding equipment and operational efficiency. We calculated the  $T_{1/2}$  values of investigated samples within the same energy spectrum using attenuation coefficients in this analysis. The variance of the half value layer ( $T_{1/2}$ ) as a feature of photon energy is shown in Figure 3.

With increasing photon energy, we found a direct improvement in the necessary glass thickness, which will result in a 50% reduction in incident photon density. This is demonstrated by the fact that the penetration properties of energetic photons shift as they progress from low to high energy levels [41]. In other terms, photons with a higher energy need tougher materials to achieve a halving of their power. However, it is necessary to equate the appropriate material thickness of various materials in order to halve the energy of a certain photon. As previously discussed, Sample 8 was reported with the maximum linear attenuation coefficients. Since there is an inverse relationship between  $T_{1/2}$  and linear attenuation coefficients (see Equation (5)), one can say that shields with higher linear attenuation coefficients can provide lower  $T_{1/2}$  values. This is supported by our observation that Sample 8 had the lowest  $T_{1/2}$  values of all the glasses studied. Similar to HVL, the term TVL ( $T_{1/10}$ ) is also a significant parameter in determining the appropriate shield thickness of a substance, since it is possible for the incoming photon intensity to be reduced to a tenth of its initial value. Consequently, this configuration function can be used for shielding products and cost effectiveness. The  $T_{1/10}$  values of investigated samples within the same energy spectrum were calculated in this analysis using attenuation coefficients. Figure 4 illustrates the variance of the tenth value layer ( $T_{1/10}$ ) as a characteristic of photon energy. A similar variation trend with HVL was reported for studied glass samples. The lowest  $T_{1/10}$  values were also reported for Sample 8.

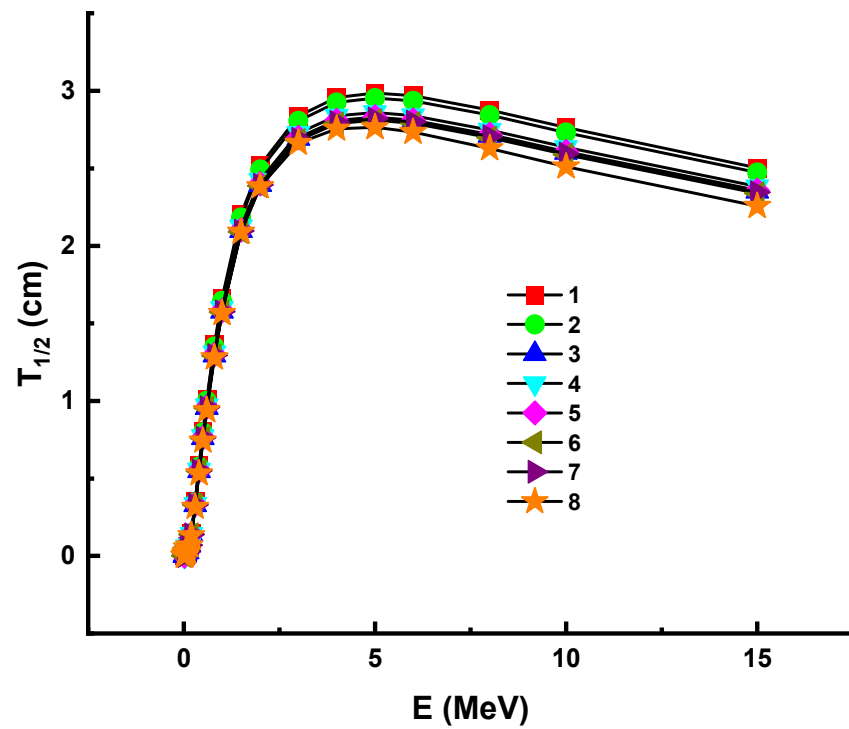


**Figure 3.** Variation of half value layer ( $T_{1/2}$ ) against photon energy for all glasses. 1— $37.5\text{Bi}_2\text{O}_3-62.5\text{B}_2\text{O}_3$ ; 2— $38\text{Bi}_2\text{O}_3-60\text{B}_2\text{O}_3-2\text{Al}_2\text{O}_3$ ; 3— $40\text{Bi}_2\text{O}_3-60\text{B}_2\text{O}_3$ ; 4— $40\text{Bi}_2\text{O}_3-59\text{B}_2\text{O}_3-1\text{Al}_2\text{O}_3$ ; 5— $40\text{Bi}_2\text{O}_3-59\text{B}_2\text{O}_3-1\text{Y}_2\text{O}_3$ ; 6— $40\text{Bi}_2\text{O}_3-59\text{B}_2\text{O}_3-1\text{Nd}_2\text{O}_3$ ; 7— $40\text{Bi}_2\text{O}_3-59\text{B}_2\text{O}_3-1\text{Sm}_2\text{O}_3$ ; 8— $40\text{Bi}_2\text{O}_3-59\text{B}_2\text{O}_3-1\text{Eu}_2\text{O}_3$ .

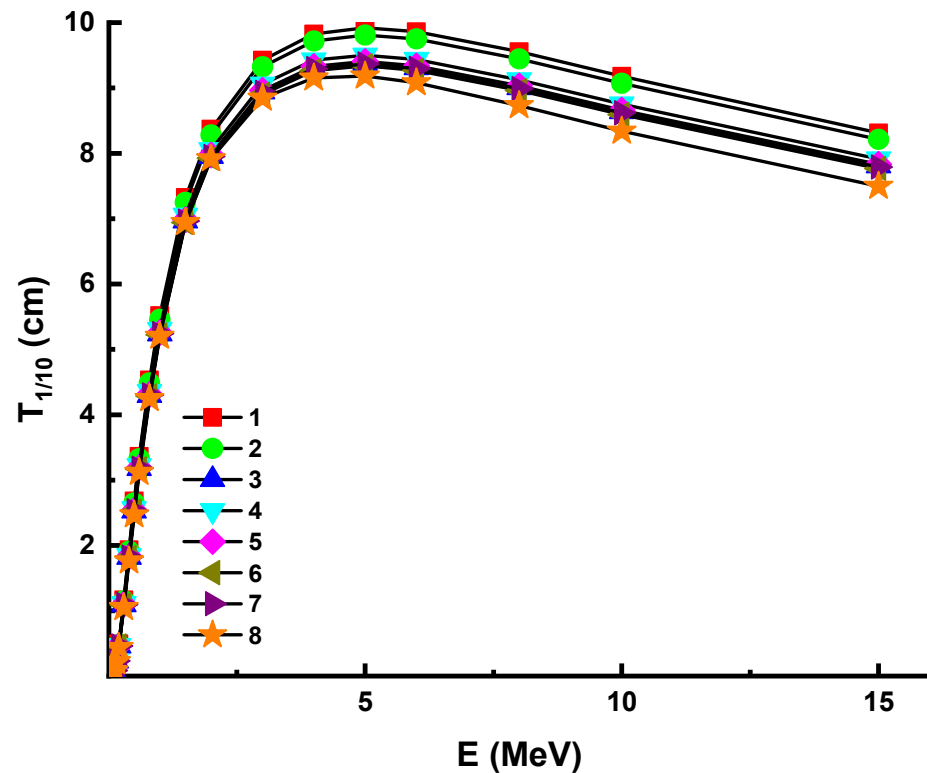


**Figure 4.** Variation of tenth value layer ( $T_{1/10}$ ) against photon energy for all glasses. 1— $37.5\text{Bi}_2\text{O}_3-62.5\text{B}_2\text{O}_3$ ; 2— $38\text{Bi}_2\text{O}_3-60\text{B}_2\text{O}_3-2\text{Al}_2\text{O}_3$ ; 3— $40\text{Bi}_2\text{O}_3-60\text{B}_2\text{O}_3$ ; 4— $40\text{Bi}_2\text{O}_3-59\text{B}_2\text{O}_3-1\text{Al}_2\text{O}_3$ ; 5— $40\text{Bi}_2\text{O}_3-59\text{B}_2\text{O}_3-1\text{Y}_2\text{O}_3$ ; 6— $40\text{Bi}_2\text{O}_3-59\text{B}_2\text{O}_3-1\text{Nd}_2\text{O}_3$ ; 7— $40\text{Bi}_2\text{O}_3-59\text{B}_2\text{O}_3-1\text{Sm}_2\text{O}_3$ ; 8— $40\text{Bi}_2\text{O}_3-59\text{B}_2\text{O}_3-1\text{Eu}_2\text{O}_3$ .



This outcome can be considered as a confirmation of the shielding effectiveness of Sample 8 in terms of halving the primary radiation intensity as well as reducing it to one tenth. MFP is the average distance traveled by photons before colliding. We determined the MFP values of studied glass samples in terms of their attenuation behaviors as a function of the average distance of an incident photon [42–44]. The difference in MFP as a function of photon energy is depicted in Figure 5 for all glasses.

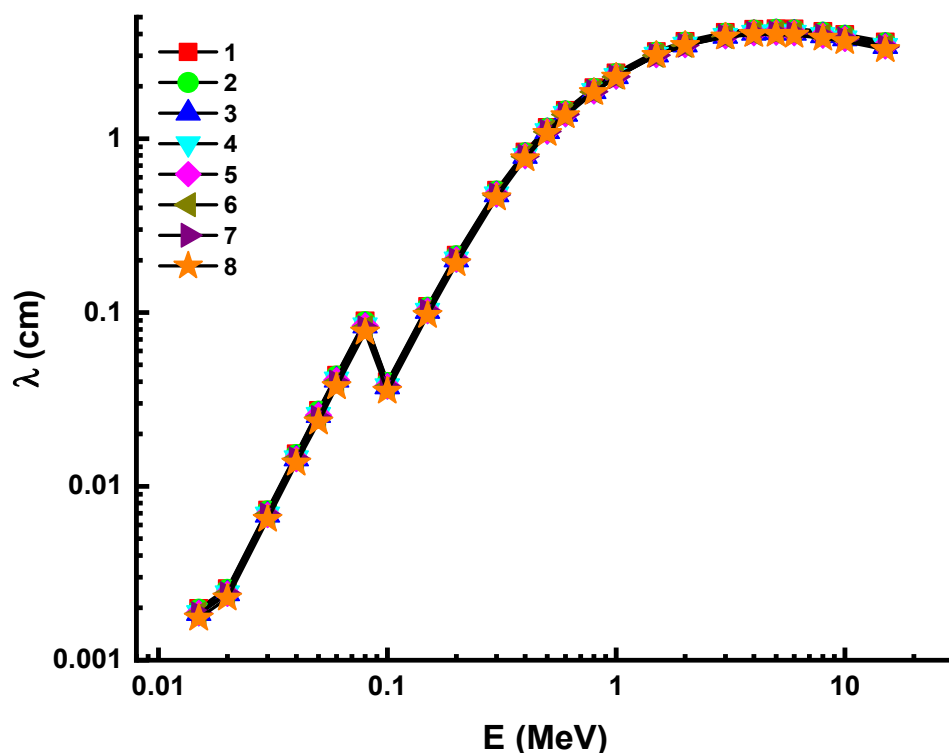


**Figure 5.** Variation of men free path ( $\lambda$ ) against photon energy for all glasses. 1—37.5Bi<sub>2</sub>O<sub>3</sub>–62.5B<sub>2</sub>O<sub>3</sub>; 2—38Bi<sub>2</sub>O<sub>3</sub>–60B<sub>2</sub>O<sub>3</sub>–2Al<sub>2</sub>O<sub>3</sub>; 3—40Bi<sub>2</sub>O<sub>3</sub>–60B<sub>2</sub>O<sub>3</sub>; 4—40Bi<sub>2</sub>O<sub>3</sub>–59B<sub>2</sub>O<sub>3</sub>–1Al<sub>2</sub>O<sub>3</sub>; 5—40Bi<sub>2</sub>O<sub>3</sub>–59B<sub>2</sub>O<sub>3</sub>–1Y<sub>2</sub>O<sub>3</sub>; 6—40Bi<sub>2</sub>O<sub>3</sub>–59B<sub>2</sub>O<sub>3</sub>–1Nd<sub>2</sub>O<sub>3</sub>; 7—40Bi<sub>2</sub>O<sub>3</sub>–59B<sub>2</sub>O<sub>3</sub>–1Sm<sub>2</sub>O<sub>3</sub>; 8—40Bi<sub>2</sub>O<sub>3</sub>–59B<sub>2</sub>O<sub>3</sub>–1Eu<sub>2</sub>O<sub>3</sub>.

It is observed that the average travel distance of an incident gamma-ray increased as photon energy increased. This can be explained by the fact that photons have different direct penetration properties depending on their initial energy. However, Sample 8 was stated to have almost the lowest MFP values across the entire range of incident photon energies. This can be explained by the atomic structure and material density of Sample 8, as its dense atomic structure prevented these gammas from passing through. Figure 6 depicts the difference in effective atomic number values due to photon radiation. Therefore, combinations with a greater percentage of Z-valued compounds have a higher absorption rate for gamma rays. According to our results, Sample 8 has the highest  $Z_{\text{eff}}$  values across all energy levels tested. However, there was no discernible difference in  $Z_{\text{eff}}$  values. This may be clarified by the fact that the molar concentrations of glass specimens vary slightly. However, the largest difference in  $Z_{\text{eff}}$  values was observed at high energy, while the highest value was observed at 0.015 MeV in the photoelectric effect's dominant region.

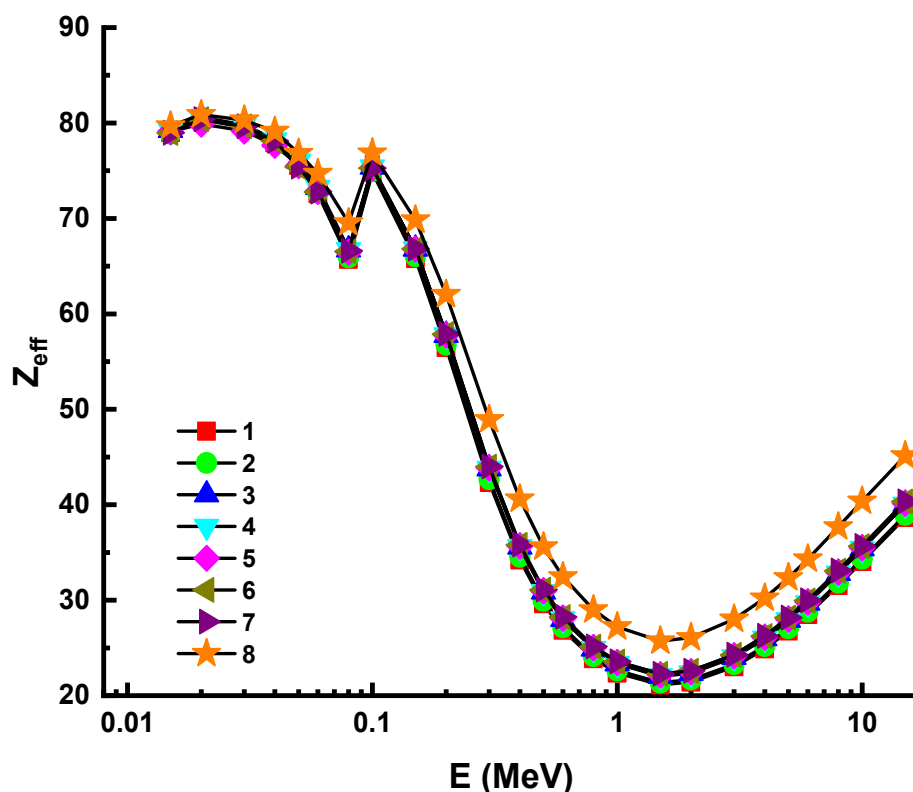


**Figure 6.** Variation of effective atomic number ( $Z_{\text{eff}}$ ) against Photon energy for all glasses. 1— $37.5\text{Bi}_2\text{O}_3-62.5\text{B}_2\text{O}_3$ ; 2— $38\text{Bi}_2\text{O}_3-60\text{B}_2\text{O}_3-2\text{Al}_2\text{O}_3$ ; 3— $40\text{Bi}_2\text{O}_3-60\text{B}_2\text{O}_3$ ; 4— $40\text{Bi}_2\text{O}_3-59\text{B}_2\text{O}_3-1\text{Al}_2\text{O}_3$ ; 5— $40\text{Bi}_2\text{O}_3-59\text{B}_2\text{O}_3-1\text{Y}_2\text{O}_3$ ; 6— $40\text{Bi}_2\text{O}_3-59\text{B}_2\text{O}_3-1\text{Nd}_2\text{O}_3$ ; 7— $40\text{Bi}_2\text{O}_3-59\text{B}_2\text{O}_3-1\text{Sm}_2\text{O}_3$ ; 8— $40\text{Bi}_2\text{O}_3-59\text{B}_2\text{O}_3-1\text{Eu}_2\text{O}_3$ .

Figure 7 illustrates the difference in effective atomic weight for absorption ( $A_{\text{eff}}$ ) as a function of photon energy for all glasses. The changes in the overall atomic weight of the mixture are directly related to the additive properties, which resulted in densities ranging from  $6.006 \text{ g/cm}^3$  to  $6.328 \text{ g/cm}^3$ . As illustrated in Figure 7, the additive types in the glass samples had an effect on the effective atomic weight for photon absorption. As a result, Sample 8 was reported to have the highest  $A_{\text{eff}}$  value of the examined glasses.

In this analysis, the EBF and EABF values were determined using the geometry progressive (G-P) method. As a result, the difference between the exposure buildup factor (EBF) and the energy absorption buildup factor (EABF) for glass samples with penetration depths of 0.5, 1, 2, 3, 4, 5, 6, 7, 8, 9, 10, 15, 20, 25, 30, and 40 mfp has been visualized in Figures 8–15. Other than the variance in EBF values, Sample 8 was determined to have the highest EBF values. In the interaction of the product and the detector material, the amount of energy in the product affects the quantity that is influenced by the amount of energy in the product and the detector function. Concerning the whole region of concentration, it is called exposure, and in the air, a detector reacts to that which is being absorbed. In EABF, the results indicated a similar attitude toward EBF; the Sample 8 EABF values were also captured as a consequence. In the 0.015–15 MeV photon energy range, the effective conductivity  $C_{\text{eff}}$  (s/m) values of the investigated glasses were finally obtained. The effective conductivity  $C_{\text{eff}}$  (s/m) of a shielding material for attenuation at room temperature (300 K) is related to the effective number of electrons. This parameter might provide useful information about investigated materials in terms of their attenuation condition at room temperature.

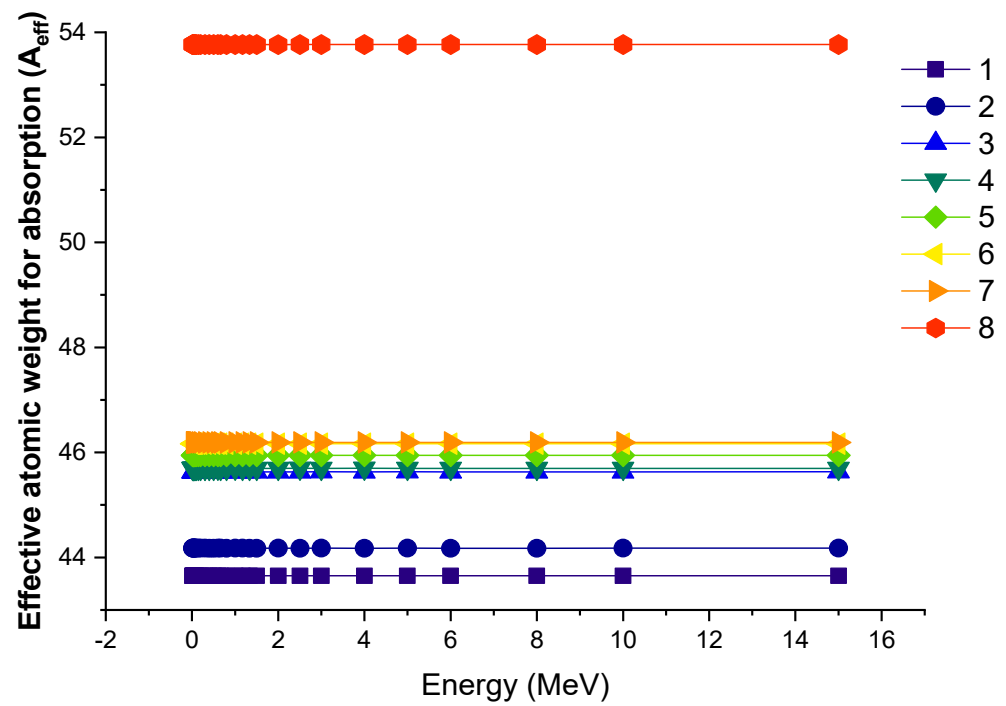


Figure 7. Variation of effective atomic weight ( $A_{eff}$ ) against photon energy for all glasses. 1— $37.5\text{Bi}_2\text{O}_3-62.5\text{B}_2\text{O}_3$ ; 2— $38\text{Bi}_2\text{O}_3-60\text{B}_2\text{O}_3-2\text{Al}_2\text{O}_3$ ; 3— $40\text{Bi}_2\text{O}_3-60\text{B}_2\text{O}_3$ ; 4— $40\text{Bi}_2\text{O}_3-59\text{B}_2\text{O}_3-1\text{Al}_2\text{O}_3$ ; 5— $40\text{Bi}_2\text{O}_3-59\text{B}_2\text{O}_3-1\text{Y}_2\text{O}_3$ ; 6— $40\text{Bi}_2\text{O}_3-59\text{B}_2\text{O}_3-1\text{Nd}_2\text{O}_3$ ; 7— $40\text{Bi}_2\text{O}_3-59\text{B}_2\text{O}_3-1\text{Sm}_2\text{O}_3$ ; 8— $40\text{Bi}_2\text{O}_3-59\text{B}_2\text{O}_3-1\text{Eu}_2\text{O}_3$ .

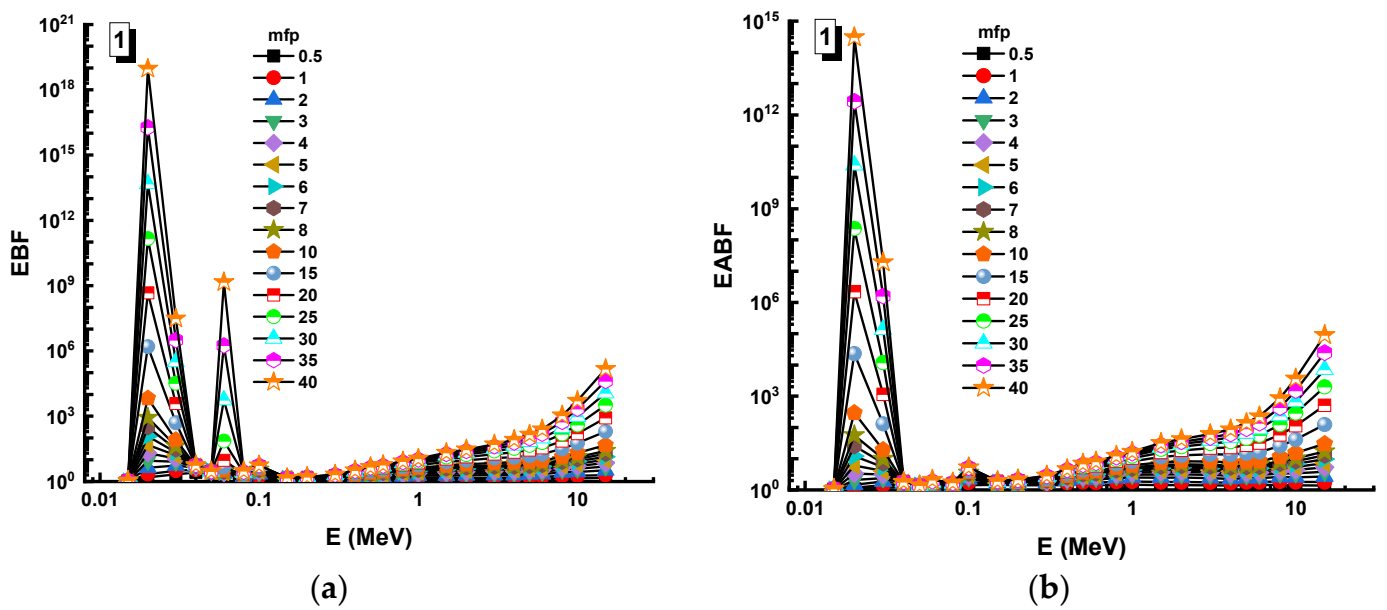


Figure 8. Variation of (a) EBF and (b) EABF against photon energy for Sample 1.

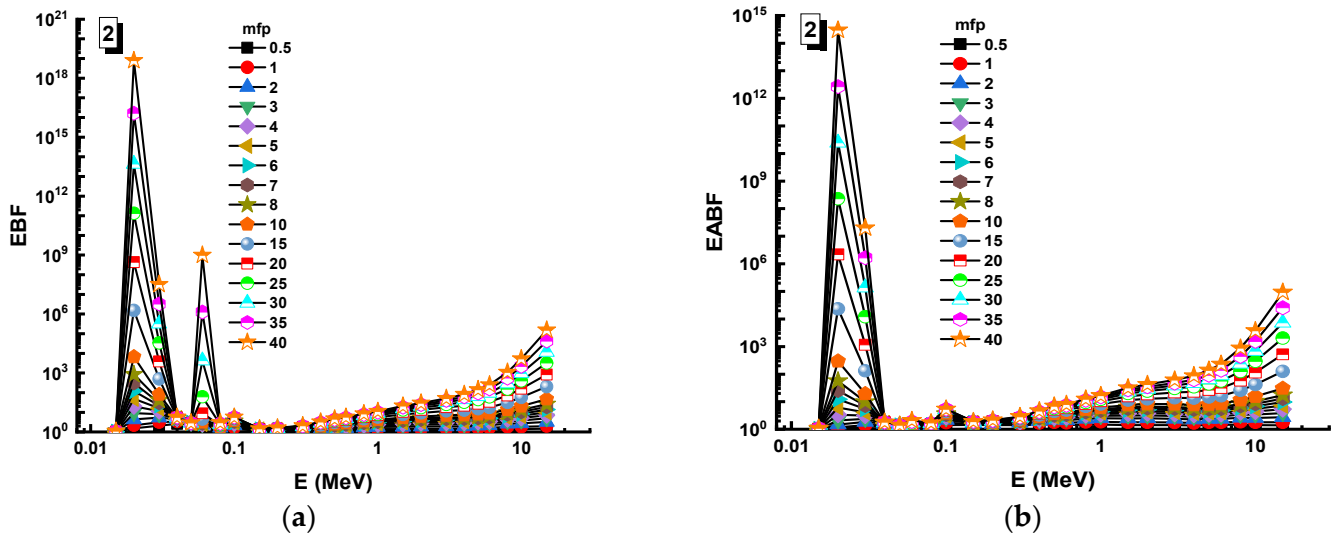


Figure 9. Variation of (a) EBF and (b) EABF against photon energy for Sample 2.

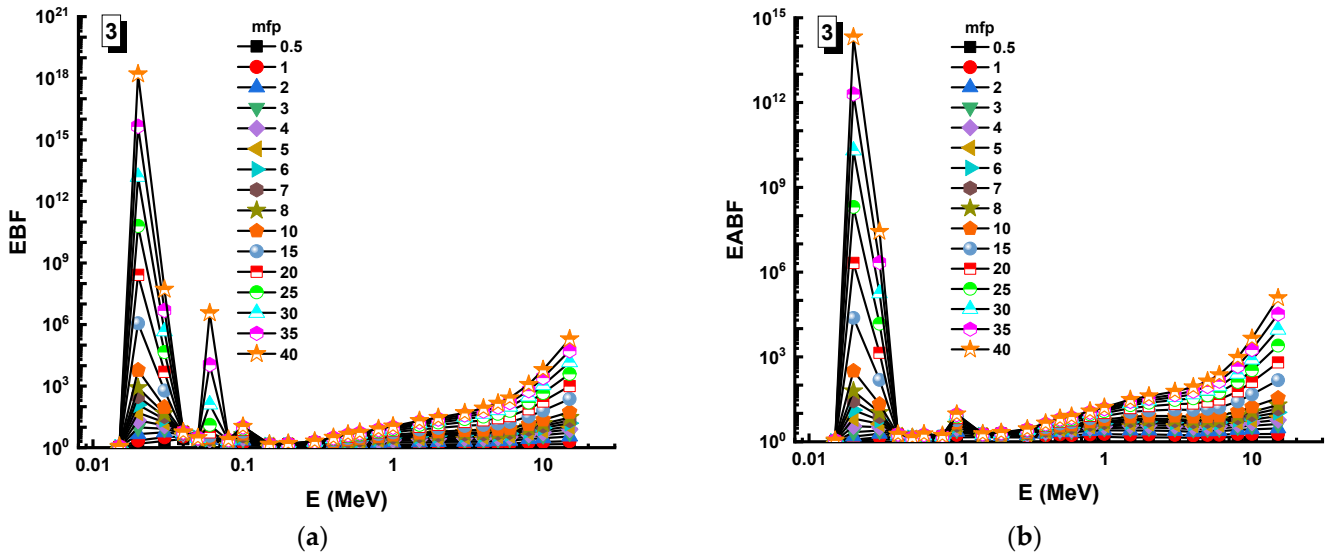


Figure 10. Variation of (a) EBF and (b) EABF against photon energy for Sample 3.

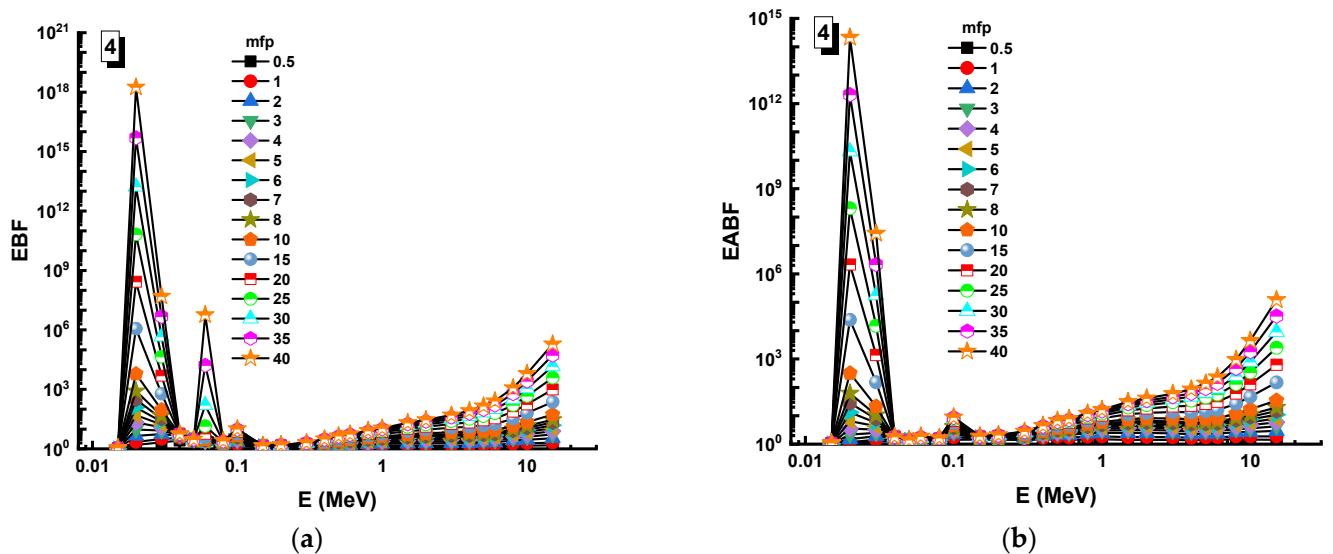


Figure 11. Variation of (a) EBF and (b) EABF against photon energy for Sample 4.

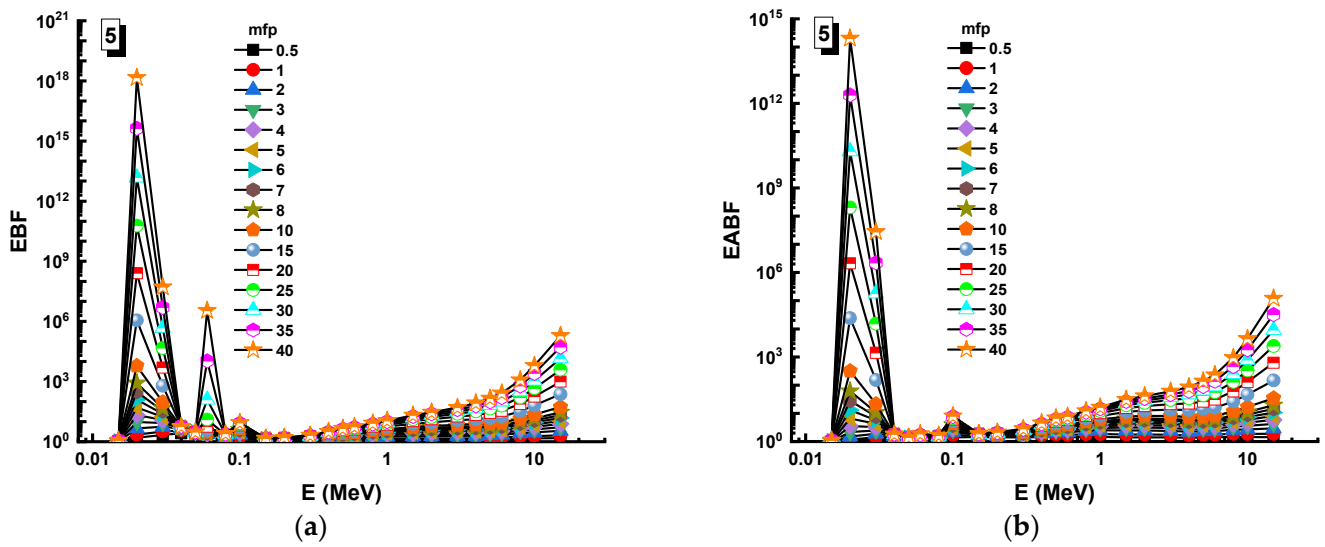


Figure 12. Variation of (a) EBF and (b) EABF against photon energy for Sample 5.

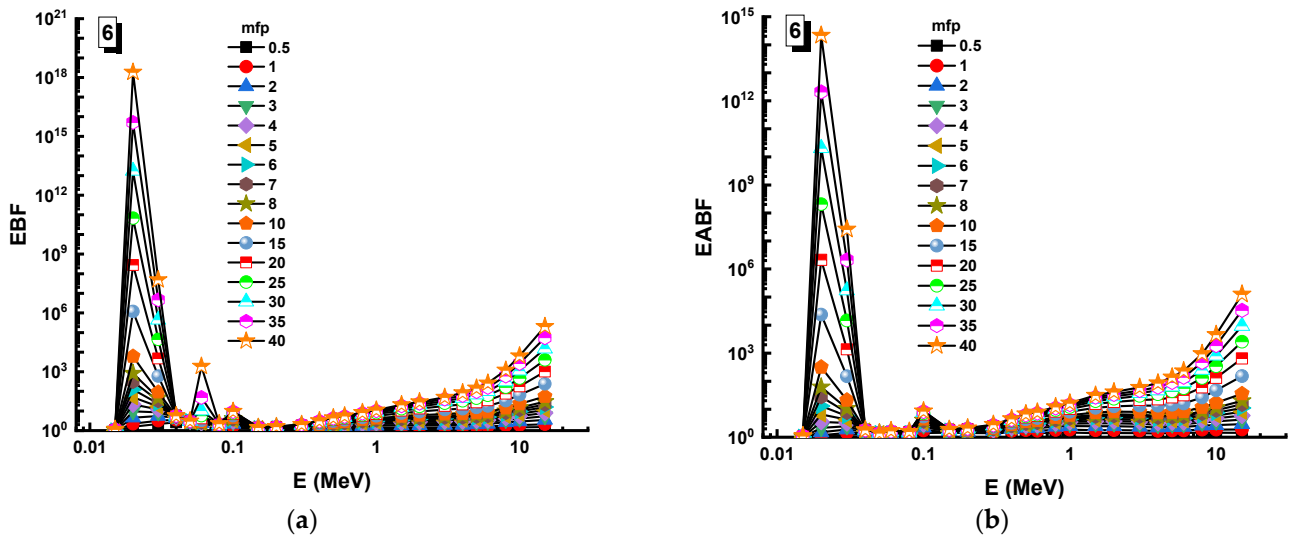


Figure 13. Variation of (a) EBF and (b) EABF against photon energy for Sample 6.

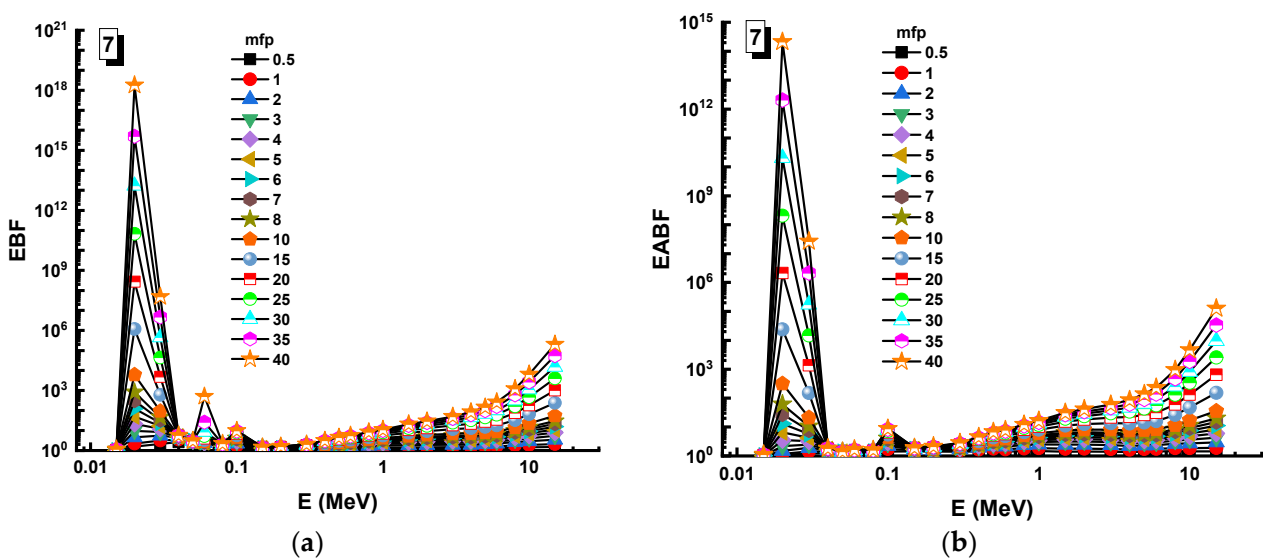


Figure 14. Variation of (a) EBF and (b) EABF against photon energy for Sample 7.

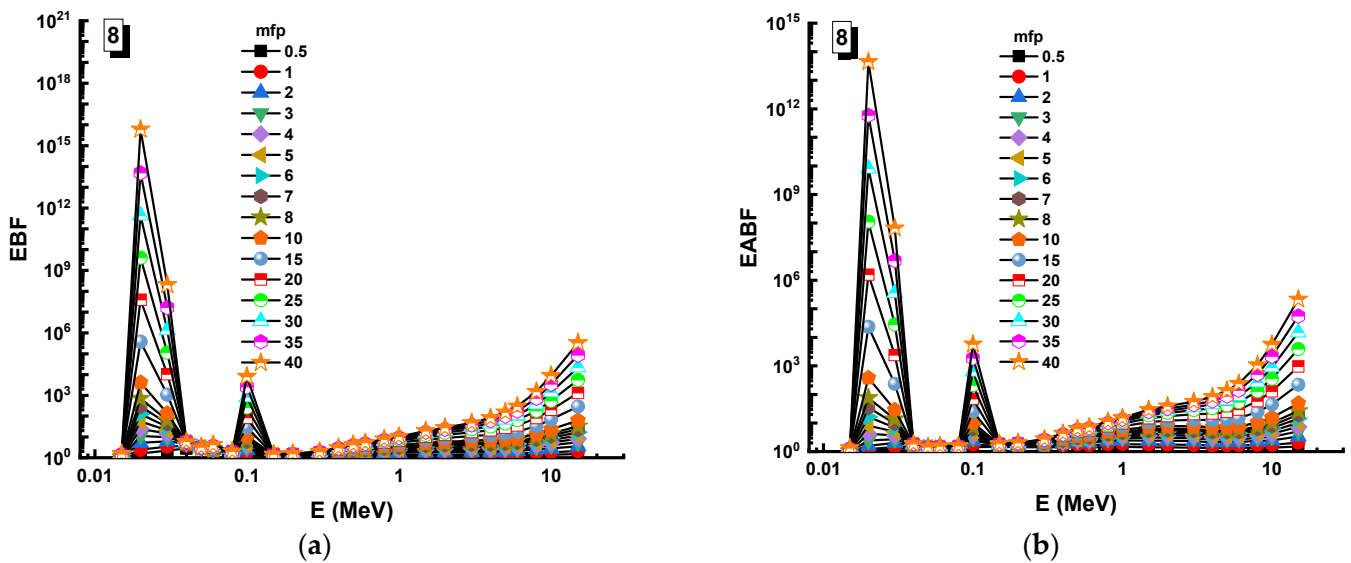


Figure 15. Variation of (a) EBF and (b) EABF against photon energy for Sample 8.

Figure 16 shows variation of effective conductivity ( $C_{eff}$ ) at 300 K (s/m) for all glasses. The results imply that as incoming photon energy rises, the effective thermal conductivity quickly falls, particularly in the low energy region, where the photoelectric effect dominates the photon–matter interaction [45,46]. However, Sample 8 was found to have the lowest  $C_{eff}$  values of all the samples examined at low energies. The findings clearly reflect that Sample 8 has the minimum heat conductivity at all photon energies, which can also be considered another beneficial feature of Sample 8 in terms of radio-protective properties

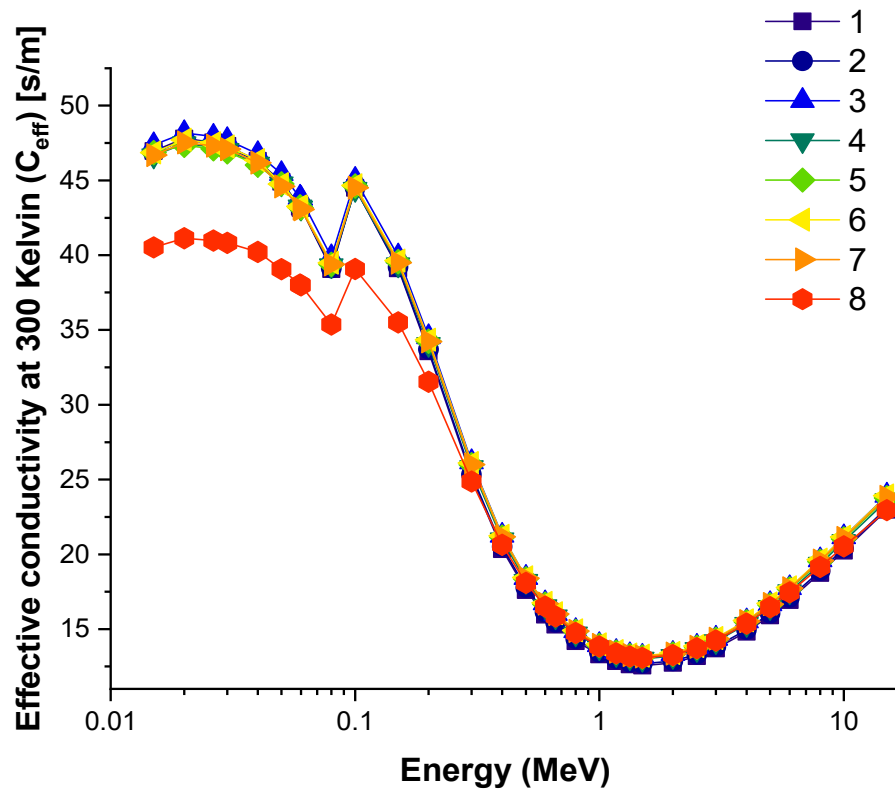


Figure 16. Variation of effective conductivity ( $C_{eff}$ ) at 300 K (s/m) for all glasses.

#### 4. Conclusions

Currently, a fascinating field of study is the fabrication of optical instruments using rare-earth element-doped materials. Rare-earth element-doped glasses are frequently used for a variety of uses, including laser materials, optical amplifiers, optical memory systems, magneto-optical instruments, surgical lasers, eye-safe lasers, flat panel displays, fluorescent lighting, and white led lasers. In addition to all these advantages, glasses doped with rare-earth oxides are used effectively in radiation shielding studies due to their high densities and their ability to decrease the number of non-bridging oxygens in the glass network that they are doped to, and thus result in a more compact structure and increased density in the newly formed material. In our study, eight different bismuth borate glasses were investigated in terms of their nuclear attenuation shielding properties, along with effective conductivity and buildup factors, for potential use in nuclear radiation facilities. Our research uncovered the following key points;

- (i) The  $\mu_m$  values of 64.49 cm<sup>2</sup>/g, 64.59 cm<sup>2</sup>/g, 65.79 cm<sup>2</sup>/g, 65.70 cm<sup>2</sup>/g, 65.87 cm<sup>2</sup>/g, 65.49 cm<sup>2</sup>/g, 65.52 cm<sup>2</sup>/g, 69.48 cm<sup>2</sup>/g were recorded for Sample 1, Sample 2, Sample 3, Sample 4, Sample 5, Sample 6, Sample 7 and Sample 8 glasses at 0.015 MeV, respectively. Generally, the  $\mu_m$  values obeyed the trend:  $(\mu_m)_8 > (\mu_m)_7 > (\mu_m)_6 > (\mu_m)_5 > (\mu_m)_4 > (\mu_m)_3 > (\mu_m)_2 > (\mu_m)_1$
- (ii) The  $T_{1/2}$  values of 2.5193 cm, 2.4923 cm, 2.3943 cm, 2.4251 cm, 2.4004 cm, 2.3857 cm, 2.3934 cm, 2.3831 cm were recorded Sample 1, Sample 2, Sample 3, Sample 4, Sample 5, Sample 6, Sample 7 and Sample 8 glasses at 2 MeV, respectively.
- (iii) The findings indicated that Sample 8 had the lowest values of MFP at the photon energies investigated.
- (iv) The findings indicate that Sample 8 has the highest  $Z_{\text{eff}}$  values at all energy levels examined.
- (v) Sample 8 was reported as having the maximum EBF and EABF values, while the minimum values were reported for the Sample 1.

From the results, it can be concluded that the effect of Eu is higher than other types of rare-earth elements such as Y, Nd, Sm and Al in terms of radiation attenuation competencies and effective conductivity at 300K. The literature review showed that researchers are considering different types of investigations in terms of adding rare-earth for nuclear radiation shielding improvements. As a result of the findings, the scientific community will be able to determine the most appropriate additive rare-earth types and glass compositions to offer the aforementioned shielding characteristics in terms of demands and usage criteria. Additionally, advanced research such as mechanical and thermal analyses of these glasses are suggested in order to get a better knowledge of their overall appropriateness for shielding applications in various kinds of radiation facilities.

**Author Contributions:** Conceptualization, G.A., H.O.T., H.M.H.Z. and S.A.M.I.; methodology, H.O.T.; software, H.O.T., H.M.H.Z., G.B. and A.E.; validation, S.A.M.I., G.K., M.A. and A.E.; formal analysis, H.M.H.Z., S.A.M.I. and A.E.; investigation, G.A., H.O.T.; resources, H.O.T., G.B. and G.K.; data curation, G.A., S.A.M.I. and A.E.; writing—original draft preparation, H.O.T., G.B. and G.K.; writing—review and editing, H.M.H.Z., M.A., S.A.M.I. and A.E.; visualization, G.A. and G.K.; supervision, H.M.H.Z., G.B. and G.K.; project administration, M.A., H.O.T. and S.A.M.I.; funding acquisition A.E. All authors have read and agreed to the published version of the manuscript.

**Funding:** The APC was covered by “Dunarea de Jos” University of Galati, Romania, through the grant no. RF3621/2021.

**Institutional Review Board Statement:** Not applicable.

**Informed Consent Statement:** Not applicable.

**Data Availability Statement:** Data is contained within the article.

**Acknowledgments:** This research was funded by the Deanship of Scientific Research at Princess Nourah bint Abdulrahman University through the Fast-track Research Funding Program.

**Conflicts of Interest:** The authors declare no conflict of interest.

## References

1. Gowda, S.; Krishnaveni, S.; Yashoda, T.; Umesh, T.K.; Gowda, R. Photon mass attenuation coefficients, effective atomic numbers and electron densities of some thermoluminescent dosimetric compounds. *Pramana* **2004**, *63*, 529–541. [[CrossRef](#)]
2. Elmahroug, Y.; Tellili, B.; Souga, C. Determination of total mass attenuation coefficients, effective atomic numbers and electron densities for different shielding materials. *Ann. Nucl. Energy* **2015**, *75*, 268–274. [[CrossRef](#)]
3. Akkurt, I.; Tekin, H.O. Radiological Parameters for Bismuth Oxide Glasses Using Phy-X/PSD Software. *Emerg. Mater. Res.* **2020**, *9*, 1020–1027. [[CrossRef](#)]
4. Ogunsola, A.; Reggiani, U.; Sandrolini, L. Modelling Shielding Properties of Concrete. In Proceedings of the 17th International Zurich Symposium on Electromagnetic Compatibility, Singapore, 27 February–3 March 2006; pp. 34–37. [[CrossRef](#)]
5. Issa, S.A.M. Effective atomic number and mass attenuation coefficient of PbO–BaO–B<sub>2</sub>O<sub>3</sub> glass system. *Radiat. Phys. Chem.* **2016**, *120*, 33–37. [[CrossRef](#)]
6. Aygün, B. High alloyed new stainless steel shielding material for gamma and fast neutron radiation. *Nucl. Eng. Technol.* **2020**, *52*, 647–653. [[CrossRef](#)]
7. William, O.-M.; John, J.F.; Danso, K.A. Assessment of radiation shielding properties of polyester steel composite using MCNP5. *Int. J. Sci. Technol.* **2012**, *2*, 455–461.
8. Alshahrani, B.; Olarinoye, I.O.; Mutuwong, C.; Sriwunkum, C.; Yakout, H.A.; Tekin, H.O.; Al-Buriahi, M.S. Amorphous alloys with high Fe content for radiation shielding applications. *Radiat. Phys. Chem.* **2021**, *183*, 109386. [[CrossRef](#)]
9. Tekin, H.O.; Kilicoglu, O. The influence of gallium (Ga) additive on nuclear radiation shielding effectiveness of Pd/Mn binary alloys. *Journal of Alloys and Compounds*, 28 September 2019, p.152484. [[CrossRef](#)]
10. Tellili, B.; Elmahroug, Y.; Souga, C. Investigation on radiation shielding parameters of cerrobend alloys. *Nucl. Eng. Technol.* **2017**, *49*, 1758–1771. [[CrossRef](#)]
11. Levet, A.; Kavaz, E.; Özdemir, Y. An experimental study on the investigation of nuclear radiation shielding characteristics in iron-boron alloys. *J. Alloys Compd.* **2020**, *819*, 152946. [[CrossRef](#)]
12. Kilic, G.; Ilik, E.; Issa, S.A.; Issa, B.; Al-Buriahi, M.S.; Issever, U.G.; Zakaly, H.M.H.; Tekin, H.O. Ytterbium (III) oxide reinforced novel TeO<sub>2</sub>–B<sub>2</sub>O<sub>3</sub>–V<sub>2</sub>O<sub>5</sub> glass system: Synthesis and optical, structural, physical and thermal properties. *Ceram. Int.* **2021**, *47*, 18517–18531. [[CrossRef](#)]
13. Kilic, G. Role of Nd<sup>3+</sup> ions in TeO<sub>2</sub>–V<sub>2</sub>O<sub>5</sub>–(B<sub>2</sub>O<sub>3</sub>/Nd<sub>2</sub>O<sub>3</sub>) glasses: Structural, optical, and thermal characterization. *J. Mater. Sci. Mater. Electron.* **2020**, *31*, 12892–12902. [[CrossRef](#)]
14. Tekin, H.O.; Alomairy, S.; Al-Buriahi, M.S.; Rammah, Y.S. Linear/nonlinear optical parameters along with photon attenuation effectiveness of Dy<sup>3+</sup> ions doped zinc-aluminoborosilicate glasses. *Phys. Scr.* **2021**, *96*, 065704. [[CrossRef](#)]
15. Kilic, G.; Issa, S.A.M.; Ilik, E.; Kilicoglu, O.; Tekin, H.O. A journey for exploration of Eu<sub>2</sub>O<sub>3</sub> reinforcement effect on zinc-borate glasses: Synthesis, optical, physical and nuclear radiation shielding properties. *Ceram. Int.* **2021**, *47*, 2572–2583. [[CrossRef](#)]
16. Kilic, G.; Issa, S.A.M.; Ilik, E.; Kilicoglu, O.; Issever, U.G.; El-Mallawany, R.; Issa, B.; Tekin, H.O. Physical, thermal, optical, structural and nuclear radiation shielding properties of Sm<sub>2</sub>O<sub>3</sub> reinforced borotellurite glasses. *Ceram. Int.* **2021**, *47*, 6154–6168. [[CrossRef](#)]
17. Tekin, H.O.; Issa, S.A.M.; Kilic, G.; Zakaly, H.M.H.; Tarhan, N.; Sidek, H.A.A.; Matori, K.A.; Zaid, M.H.M. A Systematical Characterization of TeO<sub>2</sub>–V<sub>2</sub>O<sub>5</sub> Glass System Using Boron (III) Oxide and Neodymium (III) Oxide Substitution: Resistance Behaviors against Ionizing Radiation. *Appl. Sci.* **2021**, *11*, 3035. [[CrossRef](#)]
18. Oo, H.M.; Mohamed-Kamari, H.; Wan-Yusoff, W.M.D. Optical Properties of Bismuth Tellurite Based Glass. *Int. J. Mol. Sci.* **2012**, *13*, 4623–4631. [[CrossRef](#)]
19. Mallur, S.B.; Czarnecki, T.; Adhikari, A.; Babu, P.K. Compositional dependence of optical band gap and refractive index in lead and bismuth borate glasses. *Mater. Res. Bull.* **2015**, *68*, 27–34. [[CrossRef](#)]
20. Issa, S.A.M.; Rashad, M.; Zakaly, H.M.H. Nb<sub>2</sub>O<sub>5</sub>–Li<sub>2</sub>O–Bi<sub>2</sub>O<sub>3</sub>–B<sub>2</sub>O<sub>3</sub> novel glassy system: Evaluation of optical, mechanical, and gamma shielding parameters. *J. Mater. Sci. Mater. Electron.* **2020**, *31*, 22039–22056. [[CrossRef](#)]
21. Issa, S.A.M.; Ali, A.M.; Tekin, H.O.; Saddeek, Y.B.; Al-Hajry, A.; Algarni, H.; Susoy, G. Enhancement of nuclear radiation shielding and mechanical properties of YBiO<sub>3</sub> glasses using La<sub>2</sub>O<sub>3</sub>. *Nucl. Eng. Technol.* **2020**, *52*, 1297–1303. [[CrossRef](#)]
22. Kaur, P.; Singh, K.J.; Thakur, S.; Singh, P.; Bajwa, B.S. Investigation of bismuth borate glass system modified with barium for structural and gamma-ray shielding properties. *Spectrochim. Acta Part A Mol. Biomol. Spectrosc.* **2019**, *206*, 367–377. [[CrossRef](#)]
23. Santos, D.R.S.; Santos, C.N.; de Camargo, A.S.S.; Silva, W.F.; Santos, W.Q.; Vermelho, M.V.D.; Astrath, N.G.C.; Malacarne, L.C.; Li, M.S.; Hernandez, A.C.; et al. Thermo-optical characteristics and concentration quenching effects in Nd<sup>3+</sup>-doped yttrium calcium borate glasses. *J. Chem. Phys.* **2011**, *134*, 124503. [[CrossRef](#)]
24. Guntu, R.K. Luminescence and dielectric properties of Ni<sup>2+</sup> ions added to calcio yttria borophosphate glasses for optoelectronic uses. *J. Lumin.* **2019**, *209*, 258–266. [[CrossRef](#)]
25. Kaewnuam, E.; Kim, H.J.; Jayasankar, C.K.; Chanthima, N.; Kaewkhao, J. The photoluminescence, optical and physical properties of Sm<sup>3+</sup>-doped lithium yttrium borate glasses. *Phys. Chem. Glasses—Eur. J. Glass Sci. Technol. Part B* **2016**, *57*, 85–89. [[CrossRef](#)]
26. Popov, A.I.; Lushchik, A.; Shablonin, E.; Vasil’chenko, E.; Kotomin, E.A.; Moskina, A.M.; Kuzovkov, V.N. Comparison of the F-type center thermal annealing in heavy-ion and neutron irradiated Al<sub>2</sub>O<sub>3</sub> single crystals. *Nucl. Instrum. Methods Phys. Res. Sect. B Beam Interact. Mater. At.* **2018**, *433*, 93–97. [[CrossRef](#)]



27. Kotomin, E.A.; Kuzovkov, V.N.; Popov, A.I.; Vila, R. Kinetics of F center annealing and colloid formation in Al<sub>2</sub>O<sub>3</sub>. *Nucl. Instrum. Methods Phys. Res. Sect. B Beam Interact. Mater. At.* **2016**, *374*, 107–110. [[CrossRef](#)]
28. Tucker, D.S.; Zocco, T.; Kise, C.D.; Kennedy, J.C. Effects of neutron-irradiation on MgAl<sub>2</sub>O<sub>4</sub> and Al<sub>2</sub>O<sub>3</sub>. *J. Nucl. Mater.* **1986**, *143*, 401–404. [[CrossRef](#)]
29. Mann, K.S.; Mann, S.S. Py-MLBUF: Development of an online-platform for gamma-ray shielding calculations and investigations. *Ann. Nucl. Energy* **2021**, *150*, 107845. [[CrossRef](#)]
30. Bajaj, A.; Khanna, A.; Kulkarni, N.K.; Aggarwal, S.K. Effects of Doping Trivalent Ions in Bismuth Borate Glasses. *J. Am. Ceram. Soc.* **2009**, *92*, 1036–1041. [[CrossRef](#)]
31. Mostafa, A.M.A.; Zakaly, H.M.; Al-Ghamdi, S.A.; Issa, S.A.; Al-Zaibani, M.; Ramadan, R.M.; El Agammy, E.F. PbO–Sb<sub>2</sub>O<sub>3</sub>–B<sub>2</sub>O<sub>3</sub>–CuO glassy system: Evaluation of optical, gamma and neutron shielding properties. *Mater. Chem. Phys.* **2021**, *258*, 123937. [[CrossRef](#)]
32. Issa, S.A.M.; Zakaly, H.M.H.; Pyshkina, M.; Mostafa, M.Y.A.; Rashad, M.; Soliman, T.S. Structure, optical, and radiation shielding properties of PVA–BaTiO<sub>3</sub> nanocomposite films: An experimental investigation. *Radiat. Phys. Chem.* **2020**, *180*, 109281. [[CrossRef](#)]
33. Tekin, H.O.; Sayyed, M.I.; Altunsoy, E.E.; Manici, T. Shielding properties and effects of WO<sub>3</sub> and PbO on mass attenuation coefficients by using MCNPX code. *Dig. J. Nanomater. Biostruct.* **2017**, *12*, 861–867.
34. Tekin, H.O.; Singh, V.P.; Manici, T. Effects of micro-sized and nano-sized WO<sub>3</sub> on mass attenuation coefficients of concrete by using MCNPX code. *Appl. Radiat. Isot.* **2017**, *12*, 122–125. [[CrossRef](#)] [[PubMed](#)]
35. Ali, A.M.; Issa, S.A.M.; Ahmed, M.R.; Saddeek, Y.B.; Zaid, M.H.M.; Sayed, M.; Somaily, H.H.; Tekin, H.O.; Sidek, H.A.A.; Matori, K.A.; et al. Promising applicable heterometallic Al<sub>2</sub>O<sub>3</sub>/PbO<sub>2</sub> nanoparticles in shielding properties. *J. Mater. Res. Technol.* **2020**, *9*, 13956–13962. [[CrossRef](#)]
36. Henaish, A.M.A.; Mostafa, M.; Salem, B.I.; Zakaly, H.M.H.; Issa, S.A.M.; Weinstein, I.A.; Hemeda, O.M. Spectral, electrical, magnetic and radiation shielding studies of Mg-doped Ni–Cu–Zn nanoferrites. *J. Mater. Sci. Mater. Electron.* **2020**, *22*, 20210–20222. [[CrossRef](#)]
37. El-Denglawey, A.; Zakaly, H.M.H.; Alshammari, K.; Issa, S.A.M.; Tekin, H.O.; AbuShanab, W.S.; Saddeek, Y.B. Prediction of mechanical and radiation parameters of glasses with high Bi<sub>2</sub>O<sub>3</sub> concentration. *Results Phys.* **2021**, *21*, 103839. [[CrossRef](#)]
38. Tekin, H.O.; Bilal, G.; Zakaly, H.M.H.; Kilic, G.; Issa, S.A.M.; Ahmed, E.M.; Rammah, Y.S.; Ene, A. Newly developed vanadium-based glasses and their potential for nuclear radiation shielding aims: A monte carlo study on gamma ray attenuation parameters. *Materials* **2021**, *14*, 3897. [[CrossRef](#)]
39. Zakaly, H.M.; Ashry, A.; El-Taher, A.; Abbady, A.G.E.; Allam, E.A.; El-Sharkawy, R.M.; Mahmoud, M.E. Role of novel ternary nanocomposites polypropylene in nuclear radiation attenuation properties: In-depth simulation study. *Radiat. Phys. Chem.* **2021**, *188*, 109667. [[CrossRef](#)]
40. Lakshminarayana, G.; Kumar, A.; Tekin, H.O.; Issa, S.A.M.; Al-Buriahi, M.S.; Dong, M.G.; Lee, D.; Yoon, J.; Park, T. In-depth survey of nuclear radiation attenuation efficacies for high density bismuth lead borate glass system. *Results Phys.* **2021**, *23*, 104030. [[CrossRef](#)]
41. Saudi, H.A.; Tekin, H.O.; Zakaly, H.M.H.; Issa, S.A.M.; Susoy, G.; Zhukovsky, M. The impact of samarium (III) oxide on structural, optical and radiation shielding properties of thallium-borate glasses: Experimental and numerical investigation. *Opt. Mater.* **2021**, *114*, 110948. [[CrossRef](#)]
42. Zakaly, H.M.H.; Rashad, M.; Tekin, H.O.; Saudi, H.A.; Issa, S.A.M.; Henaish, A.M.A. Synthesis, optical, structural and physical properties of newly developed dolomite reinforced borate glasses for nuclear radiation shielding utilizations: An experimental and simulation study. *Opt. Mater.* **2021**, *114*, 110942. [[CrossRef](#)]
43. Al-Buriahi, M.S.; Hegazy, H.H.; Alrashedi, F.; Olarinoye, I.O.; Algarni, H.; Tekin, H.O.; Saudi, H.A. Effect of CdO addition on photon, electron, and neutron attenuation properties of boro-tellurite glasses. *Ceram. Int.* **2021**, *47*, 5951–5958. [[CrossRef](#)]
44. Tekin, H.O.; Kassab, L.R.P.; Issa, S.A.M.; Bordon, C.D.d.; Al-Buriahi, M.S.; Delboni, F.d.P.; Kilic, G.; Magalhaes, E.S. Structural and physical characterization study on synthesized tellurite (TeO<sub>2</sub>) and germanate (GeO<sub>2</sub>) glass shields using XRD, Raman spectroscopy, FLUKA and PHITS. *Opt. Mater.* **2020**, *110*, 110533. [[CrossRef](#)]
45. Zhao, C.Y.; Lu, T.J.; Hodson, H.P.; Jackson, J.D. The temperature dependence of effective thermal conductivity of open-celled steel alloy foams. *Mater. Sci. Eng. A* **2004**, *367*, 123–131. [[CrossRef](#)]
46. Tekin, H.O.; Issa, S.A.M.; Mahmoud, K.A.; El-Agawany, F.I.; Rammah, Y.S.; Susoy, G.; Al-Buriahi, M.S.; Abuzaid, M.M.; Akkurt, I. Nuclear Radiation Shielding Competences of Barium (Ba) Reinforced Borosilicate Glasses. *Emerg. Mater. Res.* **2020**, *9*, 1131–1144. [[CrossRef](#)]